Journal of Power Sources 240 (2013) 232–240

Contents lists available at SciVerse ScienceDirect

Journal of Power Sources

journal homepage: www.elsevier.com/locate/jpowsour

Ammonia-mediated suppression of coke formation in direct-methane solid oxide fuel cells with nickel-based anodes

Wei Wang [a], Ran Ran [a], Chao Su [b], Youmin Guo [c], David Farrusseng [c], Zongping Shao [a,b,*]

[a] State Key Laboratory of Materials-Oriented Chemical Engineering, College of Chemistry & Chemical Engineering, Nanjing University of Technology, No. 5 Xin Mofan Road, Nanjing 210009, PR China
[b] Department of Chemical Engineering, Curtin University, Perth, WA 6845, Australia
[c] Institut de Recherches sur la Catalyse et l'Environnement de Lyon (IRCELYON), UMR5256, CNRS/Université Claude Bernard, Lyon 1, 2 Av. A. Einstein, F-69626 Villeurbanne, France

HIGHLIGHTS

- The addition of NH_3 could decrease the coke formation rates of Ni–YSZ anode.
- The addition of NH_3 could also decrease the coke formation rates of Ni–Al_2O_3.
- The addition of NH_3 could increase the power output of the fuel cells.
- The addition of NH_3 could improve the operational stability of the fuel cells.
- No NO_x was detected in the exhaust gas.

ARTICLE INFO

Article history:
Received 9 January 2013
Received in revised form
2 April 2013
Accepted 4 April 2013
Available online 10 April 2013

Keywords:
Solid oxide fuel cells
Methane
Ammonia
Coke formation

ABSTRACT

In this study, we report a novel approach for suppressing coke formation in direct-methane solid oxide fuel cells (SOFCs) with a conventional nickel cermet anode by simply adding ammonia to the fuel gas. Because ammonia preferentially occupies the acidic sites of the anode catalyst materials, a significant decrease in the coke formation rate is realized by introducing ammonia into the methane gas. In addition, hydrogen, a decomposition product of ammonia, also acts as an additional fuel for the SOFCs, resulting in high cell performance. At 700 °C, the coke formation rate over the Ni-YSZ anode is suppressed by 71% after the addition of 33.3% NH_3 into CH_4. Suppressed coke formation is also observed for other Ni catalysts such as Ni/Al_2O_3, a common catalyst for methane reforming that has been successfully used as the anode catalyst layer for SOFCs operating on methane, which suggests that introducing NH_3 as an additive gas is a general method for suppressing the coke formation. The addition of ammonia can also effectively improve the power output and operational stability and offers a novel means for developing new coke-resistant SOFCs operating on widely available hydrocarbons for clean power generation to realize a sustainable future.

1. Introduction

SOFCs have several outstanding properties, in addition to being fabricated from relatively inexpensive materials, they show low sensitivity to impurities in the fuel gas, very high energy efficiency and fuel flexibility [1–5]. Direct-methane SOFCs have been the subject of much research during the past decade because natural gas, which consists of mainly methane, is an abundant and widely accessible fuel and methane is also the main component of biogas, a renewable energy resource [6–9]. Unfortunately, the state-of-the-art nickel-based cermet anodes suffer from serious coke formation during operation when methane fuel is used because nickel is a good catalyst for the methane cracking reaction. Recently, tremendous efforts have been focused on the development of copper-based or perovskite-based anode materials with improved coking resistance [10,11]. However, due to the relatively low catalytic activity of these materials for methane conversion, they are not currently commercially viable.

Suppressing coke formation by introducing another gas into the fuel gas, such as steam, CO_2, O_2 and H_2, has been explored

* Corresponding author. State Key Laboratory of Materials-Oriented Chemical Engineering, College of Chemistry & Chemical Engineering, Nanjing University of Technology, No. 5 Xin Mofan Road, Nanjing 210009, PR China. Tel.: +86 25 8317 2256; fax: +86 25 8317 2242.
E-mail address: shaozp@njut.edu.cn (Z. Shao).

0378-7753/$ – see front matter © 2013 Published by Elsevier B.V.
http://dx.doi.org/10.1016/j.jpowsour.2013.04.014

previously [12–14]. However, the main purpose of the additive gas is to increase the coking resistance thermodynamically. For example, Chen et al. [12] have demonstrated that the carbon deposition on a Ni–YSZ anode of an SOFC was greatly suppressed after the addition of 10% H_2O into the methane fuel gas. Pillai et al. [13] also have demonstrated that the addition of CO_2 or air to methane can improve the SOFC stability by suppressing coke formation over the Ni-based anode. Recently, the addition of hydrogen into methane fuel gas was also demonstrated to inhibit coke formation [14]. To completely prevent the coke formation thermodynamically, however, a large amount of such additive gas is required, which could decrease the cell voltage and increase the possibility of anode oxidation. Furthermore, the presence of air or oxygen could also increase the risk of explosions.

In addition to the thermodynamics, the kinetics also played an important role in the coke formation and it might be more effective to suppress the coke formation by altering the kinetics. It was well known that the coke formation behavior of a Ni-based catalyst is strongly dependent on its surface structure and acidity [15] and catalysts with many acidic sites on the surface are prone to coke formation. Basic additives or promoters that favor water adsorption and OH surface mobility can lower the coke formation rate by neutralizing the acidity of the support [16,17]. Horiuchi et al. have studied the effect of basic metal oxides on the catalytic activity and carbon deposition properties of Ni/Al_2O_3 catalysts for CO_2 reforming of methane [18]. They found that basic metal oxides affected both the catalytic activity and coke formation rate. It was suggested that the Ni/Al_2O_3 catalyst adsorbed mostly CO_2 when a basic metal oxide was present, which could limit the CH_4 decomposition reaction rate whereas the catalyst without a basic metal oxide adsorbed mostly CH_4. It was also found that an increase in the basicity of the catalyst can enhance the coke resistance because basic oxides can promote the reaction between steam/CO_2 and solid carbon [19].

Whisker carbon is one of the most destructive forms of carbon formed in methane steam reforming over Ni-based catalysts. This type of carbon was formed by the decomposition of hydrocarbons or CO on one side of the nickel particle and the subsequent nucleation of graphitized carbon on the other side of the nickel particle [20]. The process apparently began with the formation of nickel carbide [21], which has been suggested to be the essential intermediate in the coke formation process [22]. The formation of metal carbides might lead to the development of the layered carbon intermediates that grow into filamentous carbons. These initial carbonaceous materials might be further dissolved and diffuse into the nickel particles; this process was considered to be essential for the growth of carbon whiskers [21].

One approach for controlling coke formation is based on the idea of preventing carbide formation. It was reasoned that inhibiting carbide formation on the surface could slow down coke formation because the dissolution and precipitation of carbon could most likely only occur via carbide formation. It was found that basic oxides could prevent the carbide formation. For instance, Bouarab et al. [23] have found that an MgO promoter in a SiO_2-supported catalyst acted as the specific medium for ensuring a constant feed of surface oxygen to immediately oxidize surface carbide formed from methane cracking into carbon monoxide. However, it was also found that the addition of basic oxides such as K and Ca oxides could decrease the catalytic activity of Ni-based catalysts for methane conversion [24,25].

Here, for the first time, we report a unique and facile way to suppress coke formation on direct-methane SOFCs with a Ni-based anode by simply using ammonia as an additional fuel gas. The basic ammonia could occupy acidic sites on the Ni-based anode, thus effectively reducing the coke formation kinetically. In addition, the decomposition of ammonia also provides additional hydrogen for the fuel cell. Ammonia is already available worldwide, and its use as a potential hydrogen carrier for energy applications has been proposed. As a basic gas, ammonia can occupy the acidic sites of the anode; in fact, it has been widely used as a probe molecule to detect the surface acidity of catalysts [26,27]. Because the acidic sites would be preferentially occupied by NH_3 when it was introduced into the methane fuel gas, the methane cracking reaction can be effectively inhibited, and the coke formation over the nickel catalyst is expected to be suppressed.

2. Experimental

2.1. Powder synthesis

$Ba_{0.5}Sr_{0.5}Co_{0.8}Fe_{0.2}O_{3-\delta}$ (BSCF), $Sm_{0.5}Sr_{0.5}CoO_{3-\delta}$ (SSC) and $Sm_{0.2}Ce_{0.8}O_2$ (SDC) powders were synthesized using an EDTA-citrate complexing sol–gel process. The appropriate metal nitrates were dissolved in water, and a combination of EDTA and citric acid served as the complexing agents. After stirring and heating, a clear gel was obtained, which was held at 240 °C for several hours and further calcined under static air at 950 °C (BSCF), 900 °C (SSC) and 800 °C (SDC) for 5 h to obtain the desired pure-phase oxides. The Ni/Al_2O_3 catalyst, composed of 15 wt.% nickel and 85 wt.% Al_2O_3, and the Li and La co-promoted Ni/Al_2O_3 catalyst, composed of 15 wt.% nickel, 1 wt.% Li_2O, 5 wt.% La_2O_3 and 79 wt.% Al_2O_3, were synthesized by a glycine nitrite process (GNP). Stoichiometric amounts of various metal nitrates were dissolved in deionized water to form a solution, and glycine was then added at a molar ratio of glycine to total metal cations of 2. The solution was heated on a hot plate under stirring to evaporate the water until a gel precursor was obtained. This gel precursor was then transferred to a preheated electric oven at 240 °C to initialize auto-combustion. The primary powder obtained was further calcined at 850 °C for 5 h in static air to yield the desired catalyst.

2.2. Fuel cell fabrication

The fuel cell is fabricated as follows. The anode substrates were prepared by a tape casting process. The slurry for the tape casting process was prepared by two-step ball milling. The anode substrates for the single cells were drilled from the NiO + YSZ tape with a diameter of 16 mm. The disks were then sintered at an elevated

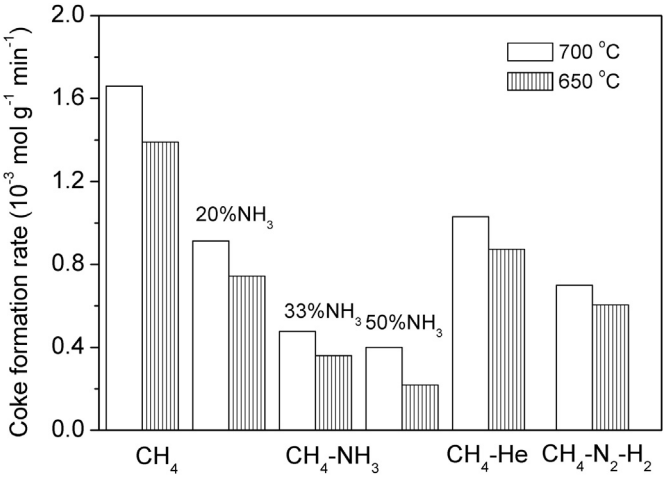

Fig. 1. Coke formation rates on the Ni-YSZ anode after treatment in CH_4-containing atmospheres for 30 min at 700 and 650 °C.

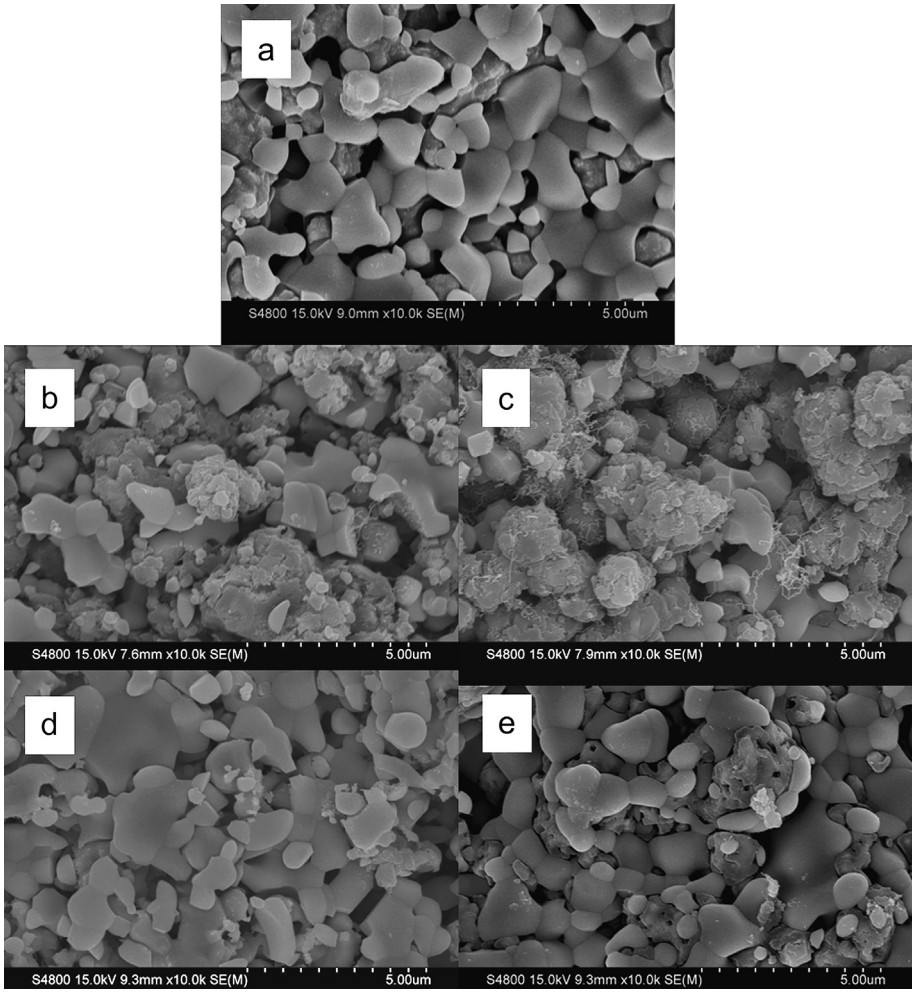

Fig. 2. SEM photos of a fresh Ni-YSZ anode (a), after treatment in pure CH_4 at 700 °C (b), after treatment in pure CH_4 at 650 °C (c), after treatment in CH_4–NH_3 (2:1) at 700 °C (d) and after treatment in CH_4–NH_3 (2:1) at 650 °C (e).

temperature for subsequent electrolyte deposition. The YSZ electrolyte layer and SDC interlayer were prepared by a wet powder spraying technique. Colloidal suspensions containing approximately 5% solid content were prepared from the YSZ and SDC powders. The colloidal suspension was then sprayed under the drive of a 1 atm nitrogen carrier gas onto the anode substrate (or YSZ) using a modified spraying gun. The cells were then sintered at 1400 °C for 5 h in air. A mixture of BSCF/SSC + SDC (7:3 in weight ratio) was used for the cathode, which was screen-printed on the central surface of the electrolyte and fired at 1000 °C in air for 2 h. A slurry of the catalyst powder was screen-painted onto the outer surface of the anode layer to form the catalyst layer and further sintered at 750 °C for 1 h. The effective area was 0.48 cm^2. In the stability test, a mesh-like morphological structure of silver paste was drawn with a stick directly onto the SSC cathode surface to create the current collector, and the electrode was subsequently fired at 180 °C for 1 h.

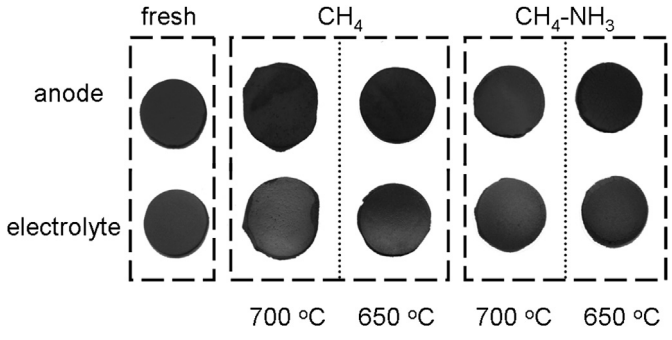

Fig. 3. Digital photos of a fresh anode and anodes after treatment in pure CH_4 or CH_4–NH_3 (CH_4:NH_3 = 2:1) for 30 min at various temperatures.

2.3. Catalytic evaluation

The catalytic activity of the anode materials and various catalysts for ammonia decomposition and methane steam reforming was studied in a flow-through, fixed-bed quartz tube reactor with

Table 1
The weight difference between the fresh cell and the cell after the treatment in pure CH_4 or CH_4:NH_3 at various temperatures.

Temperature (°C)	m_f (g)[a]	m_{t1} (g)[b]	100 $(m_f - m_{t1})/m_f$ (%)	m_f (g)	m_{t2} (g)[c]	100 $(m_f - m_{t1})/m_f$ (%)
700	0.493	0.569	15.4	0.496	0.552	11.3
650	0.493	0.556	12.8	0.490	0.523	6.73

[a] Weight of the fresh cell.
[b] Weight of the cell after the treatment in pure CH_4.
[c] Weight of the cell after the treatment in CH_4–NH_3 gas mixtures.

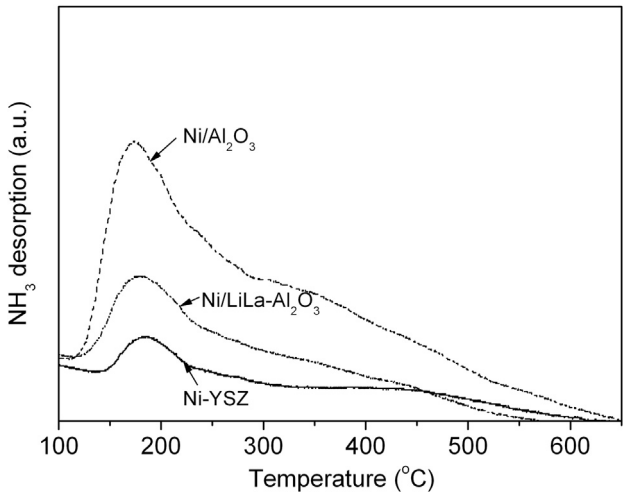

Fig. 4. NH_3-TPD profiles of the Ni-YSZ, Ni–Al_2O_3 and LiLaNi–Al_2O_3 catalysts.

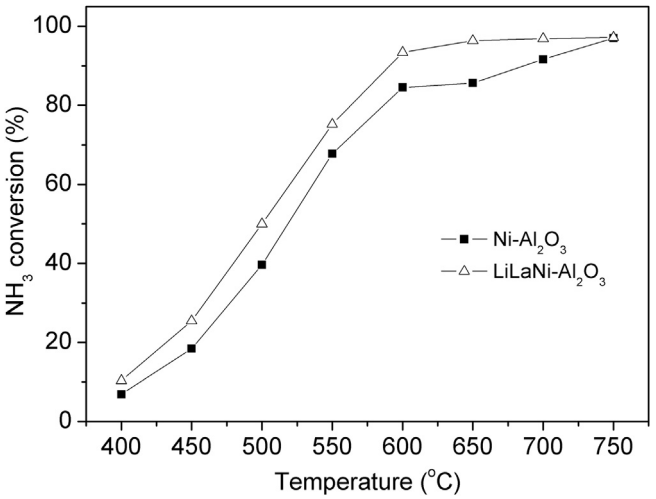

Fig. 6. Comparison of the catalytic activities of the Ni/Al_2O_3 and $Ni/LiLa–Al_2O_3$ catalysts for the NH_3 decomposition reaction.

an inner diameter of ~8 mm. The test was performed at temperatures ranging from 400 to 750 °C. Approximately 0.2 g of 40–60 mesh catalyst particles were placed in the middle of the reactor. The flow rates of ammonia, methane, steam and a diluting gas (He) were 10, 10, 10 and 80 ml min^{-1} [STP], respectively. The gas mixtures were fed into the top of the reactor, and the effluent gases at the bottom of the reactor were fed into a Varian 3800 gas chromatograph, which was equipped with Hayesep Q, Poraplot Q and 5Å sieve molecular capillary columns and a thermal conductivity detector (TCD).

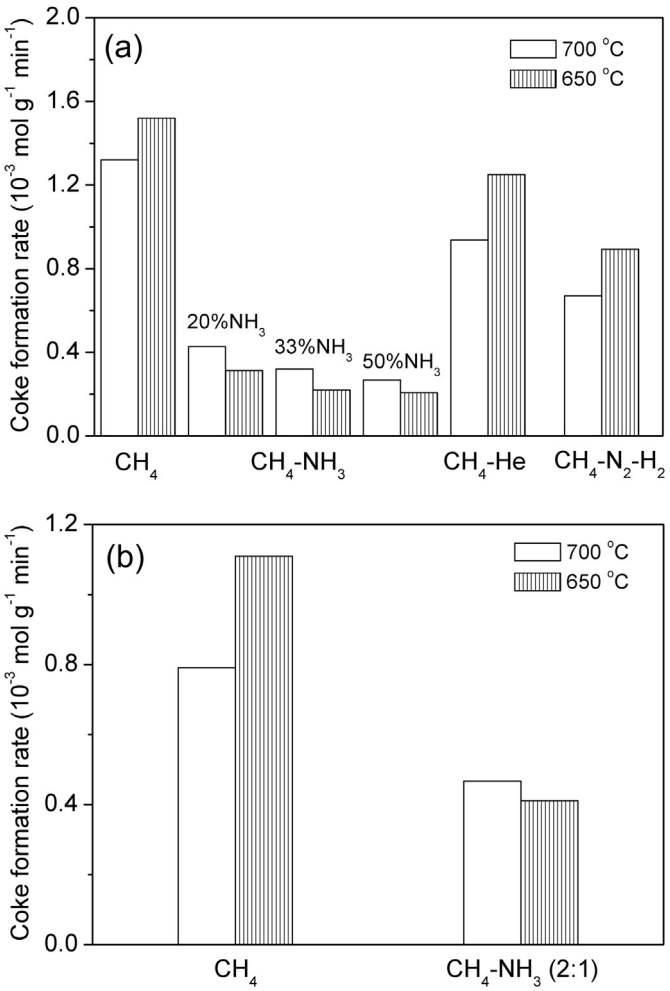

Fig. 5. Coke formation rates on the Ni/Al_2O_3 (a) and $Ni/LiLa–Al_2O_3$. (b) Catalysts after treatment in CH_4-containing atmospheres for 30 min.

2.4. Characterization

The microstructure of the fuel cells was examined with a field emission scanning electron microscopy (FESEM, Hitachi S-4800). After the catalysts were treated in a methane-containing environment for 0.5 h, the laser Raman spectra of the catalysts were collected using an HR800 UV Raman microspectrometer (JOBIN YVON, France) with the green line of an argon laser ($\lambda = 514.53$ nm) as the excitation source.

The coke resistance of the anode materials and catalysts was analyzed with oxygen temperature-programmed oxidation (O_2-TPO). Approximately 0.02 g of the anode or catalyst powder after treatment was placed into a U-type quartz reactor with an inner diameter of ~4 mm. Pure oxygen was then introduced into the

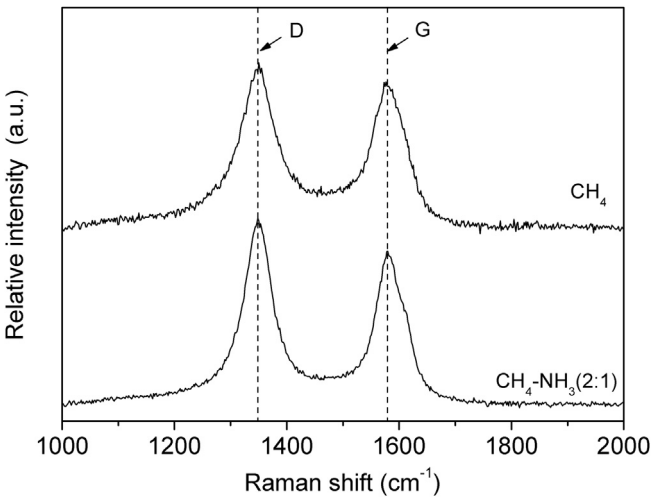

Fig. 7. Raman spectra of the carbon deposited on the Ni/Al_2O_3 catalyst after treatment in CH_4 or CH_4-NH_3.

reactor at a flow rate of 20 ml min^{-1} [STP]. The carbon deposited on the powder surface was then progressively oxidized into CO_2. The effluent gas from the reactor was fed into a Hiden QIC-20 mass spectrometer (MS) for in situ monitoring of the CO_2 concentration profile. The coke formation rates were calculated based on the CO_2 peak area in the O_2-TPO profiles. In the NH_3-TPD experiments, the samples were first treated in 10 vol.% H_2–Ar at 650 °C for 2 h, cooled to 100 °C and exposed to 5 vol.% NH_3 (30 ml min^{-1}, He in balance) for 30 min. The sample was then purged with Ar at 100 °C for 1 h and heated at 10 °C min^{-1}–650 °C. The NH_3 concentration in the effluent gas was monitored online with a BELCAT-A apparatus equipped with an in situ TCD detector.

The *I–V* and *I–P* curves of the fuel cells were obtained using a Keithley 2420 source meter based on a four-probe configuration. During the measurements, hydrogen or methane-containing fuels were fed into the anode chamber, and ambient air was used as the cathode atmosphere. The flow rate of hydrogen or methane was kept at 80 ml min^{-1} [STP], and the flow rate of NH_3 was 40 ml min^{-1} [STP] when it was fed to the anode separately. The electrode polarization resistance investigated using electrochemical impedance spectroscopy (EIS) was using a Solartron 1260 Frequency Response Analyzer in combination with a Solartron 1287 potentiostat. The frequencies used for EIS measurements ranged from 0.1 to 1000 kHz, and the signal amplitude was 30 mV.

3. Results and discussion

3.1. Carbon deposition

We first employed O_2-TPO to evaluate the coke formation over the Ni-YSZ anodes after exposure to various methane-containing atmospheres at elevated temperatures. The coke formation rates at different conditions were calculated based on the CO_2 peak area of the O_2-TPO profiles, and the results are shown in Fig. 1. At 700 °C, the coke formation rate over the Ni-YSZ anode was suppressed by 55% after the addition of 25% ammonia into the methane fuel. To determine how the dilution of the fuel with NH_3 affected the coke formation, we also investigated the coke formation rate over the

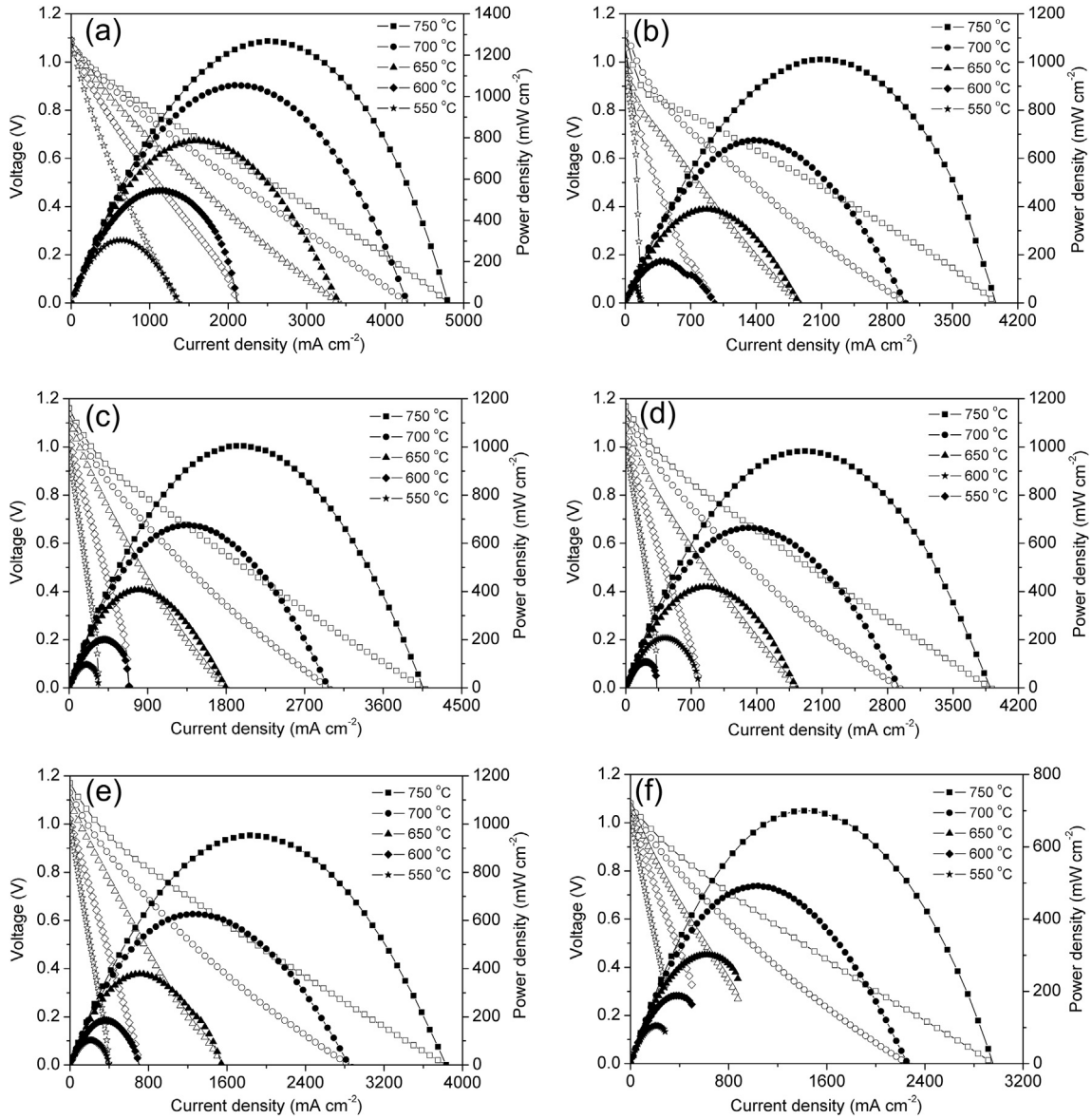

Fig. 8. *I–V* and *I–P* curves for the fuel cell (Ni-YSZ/YSZ/SDC/BSCF + SDC) operating on various 3% water humidified fuels. H_2 (a), CH_4 (b), 80% CH_4+20% NH_3 (c), 66.7% CH_4+33.3% NH_3 (d), 50% CH_4+50% NH_3 (e) and pure NH_3 (f).

Ni-YSZ anode with inert helium as the diluting agent instead of NH_3. The coke formation rate decreased only slightly with the introduction of helium into the methane fuel gas. Because NH_3 could effectively decompose at high operational temperatures, the coke formation on Ni-YSZ was also evaluated under a gas mixture composed of 50% CH_4, 37.5% H_2 and 12.5% N_2. It was found that the addition of hydrogen can suppress the coke formation somewhat and the amount of coke formed was less than that formed in the presence of the CH_4–He (2:1) mixture but greater than that formed in the presence of the CH_4–NH_3 (2:1) mixture. These results suggested that the hydrogen produced by the decomposition of NH_3 can also suppress the coke formation, which was consistent with the literature [14].

The suppression of the coke formation due to the addition of ammonia was more clearly demonstrated by the SEM images of the Ni-YSZ anode surface after exposure to CH_4 or CH_4–NH_3 gas mixtures. As shown in Fig. 2, filamentous carbon was observed on the anode after the treatment in pure methane at 700 and 650 °C (Fig. 2b and c), while there was almost no coke formation over the Ni-YSZ cermet anode after the treatment with methane gas containing 33.3% NH_3 at the same conditions (Fig. 2d and e). The ability of NH_3 to suppress coke formation over Ni-YSZ was also supported by the differences in the geometric changes in the cells after the treatment in the CH_4 and CH_4–NH_3 atmospheres under open-circuit conditions (Fig. 3). Serious deformation of the anode disk was observed for the cell after the treatment in pure CH_4 at 650 and 700 °C for 30 min, while the cell retained nearly the same morphology as the fresh one after the treatment in the CH_4–NH_3 gas mixture. The weight difference between the fresh cell and the cell after the treatment in CH_4 or CH_4–NH_3 was listed in Table 1. The cell weight increased by 12.8% after the treatment at 650 °C in pure CH_4, while the cell gained only 6.73% in weight after the treatment in the 33.3% NH_3–66.7% CH_4 gas mixture.

Suppressed coke formation was also observed for other Ni catalysts such as Ni/Al_2O_3, a common catalyst for methane reforming that has also been successfully used as an anode catalyst layer for SOFCs operating on methane [28]. These results suggest that NH_3 can be used as an additional fuel gas in a broad range of SOFCs to suppress the coke formation. As demonstrated by the NH_3-TPD profiles shown in Fig. 4, the Ni/Al_2O_3 catalyst had a much higher content of acid sites than Ni-YSZ. Shown in Fig. 5a are the coke formation rates on the Ni/Al_2O_3 catalyst under various methane-containing atmospheres. The decrease in the coke formation rate on the Ni/Al_2O_3 catalyst was also dramatic. For example, at 650 °C, the coke formation rate was reduced by 79% with the addition of 25% NH_3, and the coke formation rate continued to decrease noticeably with an increase in the NH_3 content to 33.3%. By introducing ammonia into methane gas, the coke formation rate over the Ni/Al_2O_3 catalyst was even lower at 650 °C than at 700 °C, which was significantly different from the coke formation rate behavior in pure methane. It is well known that Ni/Al_2O_3 can catalyze the decomposition of NH_3; therefore, the actual NH_3 concentration in the fuel gas should be different from that in the initial gas mixture. As shown in Fig. 6, the remaining ammonia content in the fuel gas was higher at 650 °C than at 700 °C. Thus, the preferential occupation of the acidic sites of the Ni/Al_2O_3 catalyst by ammonia became more significant at the lower temperature, which explained the larger decrease in the coke formation rate at lower temperatures when NH_3 was added to the methane fuel gas.

To further support the importance of the preferential occupation of acidic sites by ammonia for suppressing coke formation, we also synthesized a $Ni/LiLa–Al_2O_3$ catalyst and compared its coke formation rate with and without the presence of ammonia in the methane fuel gas using the same conditions as those used for Ni/Al_2O_3. Previously, we have demonstrated that the introduction of La and Li oxide promoters into Ni/Al_2O_3 increased the coke resistance for operating on methane due to the improved surface basicity as shown in Fig. 4. As shown in Fig. 5b, the coke formation rates of the $Ni/LiLa–Al_2O_3$ catalyst at 650 and 700 °C were both lower than those of Ni/Al_2O_3 when operating on pure methane as expected. However, with the addition of 33.3% NH_3 into the methane gas, the coke formation rates of $Ni/LiLa–Al_2O_3$ were 87% and 46% higher than those of Ni/Al_2O_3 at 650 and 700 °C, respectively. It was reported that adding the lanthanide promoters to Ni/Al_2O_3 could improve its catalytic activity for ammonia decomposition [29]. We also found that $Ni/LiLa–Al_2O_3$ had higher catalytic activity for NH_3 decomposition than Ni/Al_2O_3. As shown in Fig. 6, the ammonia conversions were 96.9 and 96.3% at 650 and 700 °C, respectively, for the $Ni/LiLa–Al_2O_3$ catalyst, which were higher than those for Ni/Al_2O_3 (91.6% and 85.6%). Thus, more of the acidic sites on $Ni/LiLa–Al_2O_3$ were unoccupied compared to those on Ni/Al_2O_3 due to the lower NH_3 concentration in the atmosphere. The above results imply that ammonia in the fuel gas is more effective than basic elements (Li and La) in the catalyst surface at suppressing the coke formation during the SOFC operation on methane.

Because the coke formation is dynamic, the amount of carbon formed is also closely related to the ease at which dynamically formed carbon can be eliminated during the operation. It is well known that carbon has several structures with different capacities for gasification. Raman spectroscopy provides a useful technique for detecting the structures of deposited carbon [30]. As shown in Fig. 7, there are two main bands (D and G) in the Raman spectra. It

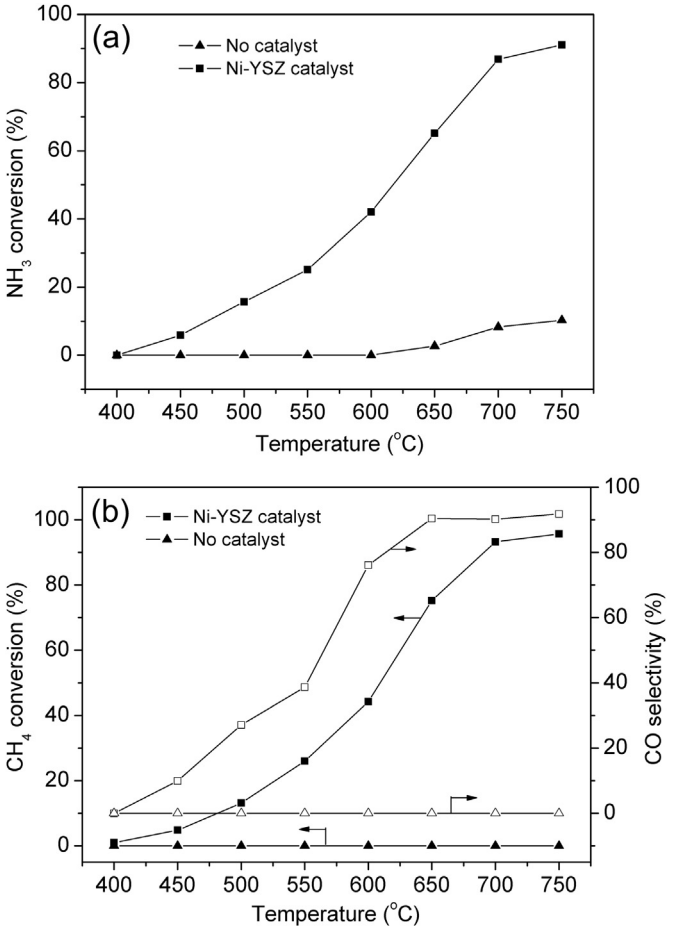

Fig. 9. Catalytic activity for ammonia decomposition (a) and methane steam reforming (b) without the catalyst and with the Ni-YSZ anode.

was reported that the graphitization degree of carbon was closely related to the integrated intensity ratio of the D to G bands, R (I_D/I_G), and a smaller *R* value indicates a higher graphitization degree of the carbon [31]. The *R* values of the deposited carbon treated in CH_4 and CH_4–NH_3 were 1.05 and 1.29, respectively, suggesting that the addition of ammonia also effectively decreased the graphitization degree of the deposited carbon. In other words, the carbon deposited in the presence of the CH_4–NH_3 mixture was easier to eliminate.

3.2. Cell performance

The dissociative adsorption and diffusion processes of hydrogen on metal surface sites were studied by some researchers using dry and moist fuel gases [32,33]. It was found that the hydrogen dissociation is very fast at the SOFC operating temperature; however, the coverage of adsorbed hydrogen species is very low. Thus, the surface diffusion process on metal surfaces is the rate-limiting process. In moist hydrogen, the overall reaction rate increases due to the competitive adsorption of oxygen from the dissociation of water and the significantly faster surface diffusion by spillover, although the sites for hydrogen dissociation on the Ni surface decrease in the case of wet hydrogen [32,33]. In the slightly humidified methane fuel, i.e., 3 vol.% H_2O, the addition of a small amount of steam could induce the steam reforming of methane to produce H_2 and CO, thereby improving the cell performance, since because H_2 and CO have a much higher electrochemical oxidation rate than methane over nickel anodes. In fact, this small amount of H_2O could not affect the coke formation behavior significantly.

Fig. 8 shows the current–voltage (*I*–*V*) and current–power (*I*–*P*) curves of a cell with a Ni-YSZ cermet anode operating on various 3% H_2O humidified fuels. The cell with hydrogen fuel delivered peak power densities (PPDs) of 304, 544, 785, 1054 and 1267 mW cm^{-2} at 550, 600, 650, 700 and 750 °C, respectively. When the fuel was switched to methane, the PPD decreased considerably at all of the operation temperatures due to the

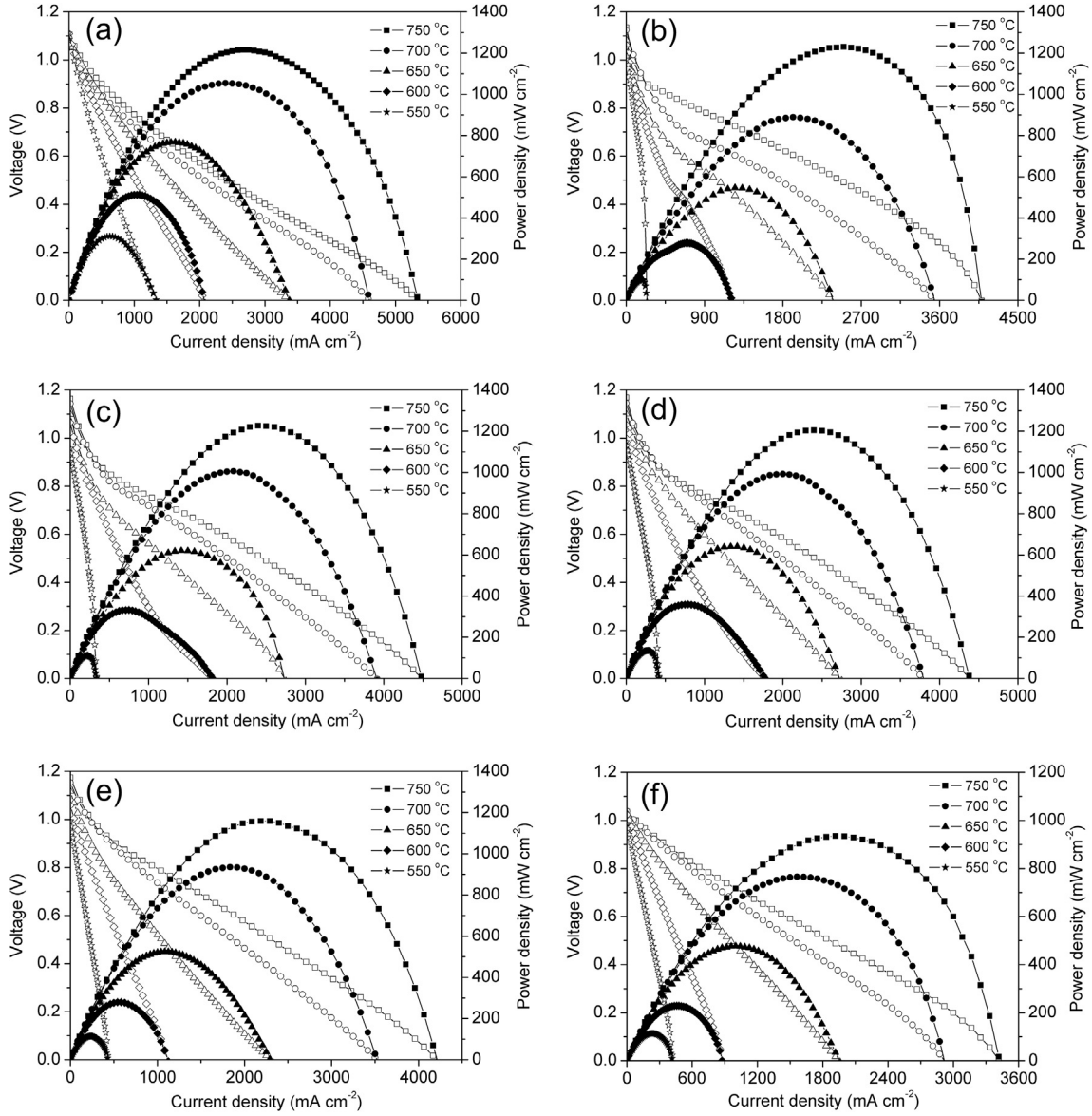

Fig. 10. *I*–*V* and *I*–*P* curves for the fuel cell (Ni/Al_2O_3/Ni-YSZ/YSZ/SDC/BSCF + SDC) operating on various 3% H_2O humidified fuels. H_2 (a), CH_4 (b), 80% CH_4 + 20% NH_3 (c), 66.7% CH_4 + 33.3% NH_3 (d), 50% CH_4 + 50% NH_3 (e) and pure NH_3 (f).

relatively low catalytic activity of Ni-YSZ for methane conversion. The *I–V* and *I–P* curves of the cell with different methane to ammonia ratios and pure ammonia as fuels were also presented (Fig. 8). Adding an appropriate amount of ammonia (less than 33.3%) to the fuel gas did not affect the PPDs significantly. However, excessive amounts of ammonia decreased the power output at higher temperatures due to the diluting effect of the NH_3 decomposition product, N_2, in the anode chamber. At temperatures below 600 °C, the PPDs were relatively higher when ammonia was present because the catalytic activity of Ni-YSZ for ammonia decomposition was better than that for methane steam reforming at reduced temperatures (Fig. 9).

To further improve the power output, we applied Ni/Al_2O_3 onto the anode as a catalyst layer. Fig. 10 shows the *I–V* and *I–P* curves of the cell with the Ni/Al_2O_3 catalyst layer operating on various 3% H_2O humidified fuels. The cell with hydrogen fuel delivered PPDs of 311, 512, 768, 1052 and 1215 mW cm^{-2} at 550, 600, 650, 700 and 750 °C, respectively, which were comparable to those of the cell without the catalyst layer (Fig. 8). When the fuel gas was switched to methane, the PPD at 750 °C was very close to that of hydrogen, demonstrating the effectiveness of Ni/Al_2O_3 in improving the cell performance. The good cell performance on methane fuel can be explained by the good activity of Ni/Al_2O_3 for methane steam reforming [28]. The *I–V* and *I–P* curves of the cell with different methane to ammonia ratios and pure ammonia as fuels were also presented (Fig. 10). The addition of ammonia (25% and 33.3%) was found to further improve the cell performance, and this beneficial effect was more noticeable above 600 °C. The improved cell performance can be explained by the good catalytic activity of Ni/Al_2O_3 for ammonia decomposition and by the higher oxidation rate of the NH_3 decomposition product, H_2, over the anode than that of methane. The PPDs were 546, 617, 640, 530 and 477 mW cm^{-2} for operating on CH_4, CH_4–NH_3 (4:1), CH_4–NH_3 (2:1), CH_4–NH_3 (1:1) and NH_3, respectively (Fig. 11a). Again, excessive ammonia had a negative effect on the power output due to the diluting effect of N_2 produced in the fuel. The cell operating on the CH_4–NH_3 (2:1) fuel delivered the highest power output, which was 17% higher than that of the cell without the ammonia addition. The area-specific resistances of the fuel cell were determined from the impedance spectra. In EIS, the high-frequency offset on the real axis is primarily a result of the resistance of the electrolyte, whereas the difference between the high and low frequency intercepts on the real axis is associated with the electrode contribution, which includes both the anode and the cathode. Because the same cell was used for operation on various fuels, so the difference between the electrode polarization resistances operating on the various fuels should originate solely from the anode. In our previous work, we found that the electrode polarization resistance increased when the fuel gas was changed from H_2 to CH_4–CO_2 while the PPDs for the H_2 and CH_4–CO_2 fuels were very similar [34]. We further studied the impedance spectra of the fuel cell operating on the CH_4–CO_2 gas mixture and pure hydrogen as fuels at 0.7 V, and found that the electrode polarization resistances of CH_4–CO_2 and H_2 became almost the same under polarization. Under polarization, O^{2-} was transferred from the cathode side to the anode side of the cell, which reacted with methane to increase the syngas concentration in the anode chamber; another important reaction is the reforming of methane with H_2O produced by the cell discharge, as a result, the electrode performance was increased [34]. Thus, in this study, we have studied the impedance spectra of the fuel cell operating on various fuels at 0.7 V, which was shown in Fig. 11b. As shown in this figure, the fuel cell with CH_4–NH_3 (2:1) fuel showed the lowest electrode polarization resistance and the fuel cell with NH_3 fuel presented the largest one, which was in good agreement with the results in Fig. 11a. The difference in

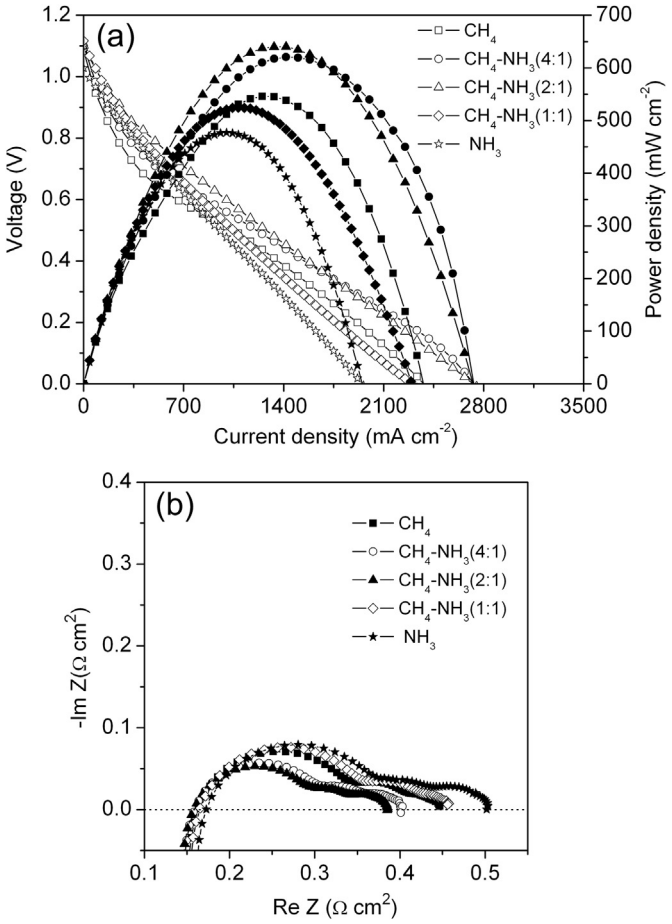

Fig. 11. A comparison of the power outputs (a) and electrode polarization resistances at 0.7 V (b) Of the fuel cells operating on the various 3% H_2O humidified fuels at 650 °C.

electrolyte resistance could be attributed to the different endothermic reactions involved in the anode chamber. Because Ni/Al_2O_3 is also prone to coke formation, the introduction of ammonia into methane was also found to be beneficial for improving the cell operational stability.

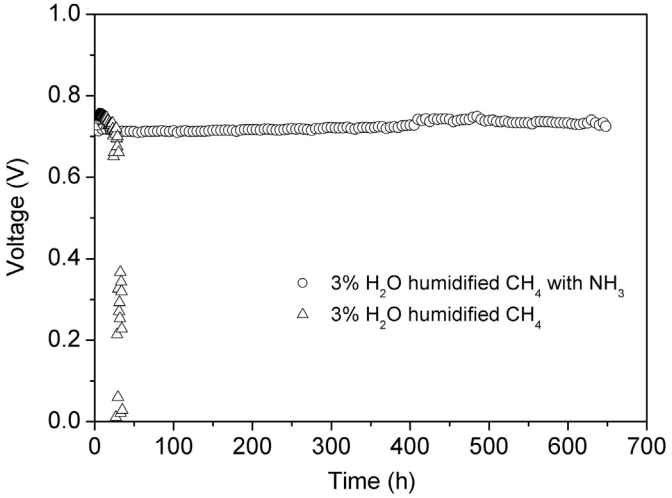

Fig. 12. The time dependence of the voltage of the fuel cell (Ni/Al_2O_3/Ni-YSZ/YSZ/SDC/SSC + SDC) operating on 3% H_2O humidified CH_4 with and without 33.3% NH_3 under a specific current density (200 mA cm^{-2}) at 650 °C.

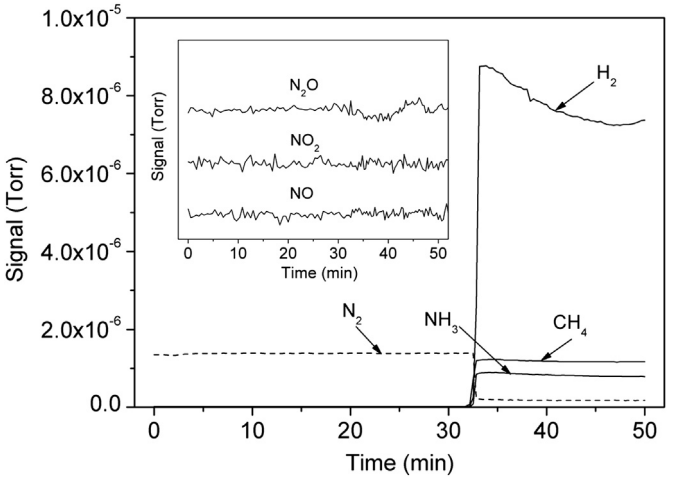

Fig. 13. The exhaust gas of the fuel cell with the Ni/Al_2O_3 catalyst layer operating on CH_4–NH_3 (2:1) under a certain current density of 200 mA cm^{-2}. The figure inset shows the detailed information of the NO_x signals because the NO_x signals are very low compared to those of the other gases.

3.3. Operational stability

To determine the effect of NH_3 on the cell operational stability, which is critical for practical applications, two similar fuel cells were first polarized under a constant current density of 300 mA cm^{-2} for 24 h at 650 °C by operating on hydrogen fuel to obtain a stable performance, and then the stability tests were conducted by operating on 3% H_2O humidified CH_4 with and without 33.3% NH_3. To avoid the possible CO_2 poisoning and the possible phase transition of the BSCF cathode, we adopted SSC as cathode material for this study instead. Fig. 12 showed the time dependence of the voltage under a current density of 200 mA cm^{-2}. For the cell without the NH_3 additive, the voltage was stable for only 20 h, and the cell eventually failed after 35 h. In contrast, the cell operation was stable for 650 h when NH_3 was added to the methane fuel gas. This significant improvement in the operational stability is clearly due to the suppressed coke formation after the introduction of ammonia into the fuel gas.

3.4. Exhaust gas analysis

It was reported that toxic NO_x might be produced under the current density in ammonia-fueled SOFCs based on an oxygen-ion conducting electrolyte [35]. To investigate the possible formation of NO_x when NH_3 was introduced into the methane fuel gas, the exhaust gas of an SOFC operating on the CH_4–NH_3 gas mixture was also monitored by an online mass spectrometer. It was found the concentration of NO_x is four orders of magnitude lower than that of N_2, suggesting that the yield of NO_x is negligible. As shown in Fig. 13, no change in the absolute intensity of the NO_x signals was observed when the atmosphere was switched from air to the exhaust gas of the SOFC under a certain polarization current of 200 mA cm^{-2}. The relatively low operation temperature of this study might account for the negligible formation of NO_x.

4. Conclusions

In conclusion, we reported an inhibition in coke formation mediated by an ammonia additive in direct-methane SOFCs without any external reforming process in this study. The addition of ammonia effectively improved the power output and operational stability on methane fuel at intermediate temperatures. This concept can be applied to many types of hydrocarbon fuels, allowing for the design of flexible SOFC systems for various applications. The SOFCs used in this paper can be easily fabricated using cost-effective methods and materials. This study presents a novel approach for developing new coke-resistant SOFCs operating on widely available hydrocarbons for clean power generation to realize a sustainable future.

Acknowledgements

This work was supported by the “National Science Foundation for Distinguished Young Scholars of China” under contract no. 51025209. Dr. Zongping Shao also acknowledges the ARC future fellowship (FT100100134).

References

[1] S. Park, J.M. Vohs, R.J. Gorte, Nature 404 (2000) 265–267.
[2] T. Hibino, A. Hashimoto, T. Inoue, J. Tokuno, S. Yoshida, M. Sano, Science 288 (2000) 2031–2033.
[3] Z.P. Shao, S.M. Haile, J. Ahn, P.D. Ronney, Z.L. Zhan, S.A. Barnett, Nature 435 (2005) 795–798.
[4] Z.L. Zhan, S.A. Barnett, Science 308 (2005) 844–847.
[5] Z.P. Shao, C.M. Zhang, W. Wang, C. Su, W. Zhou, Z.H. Zhu, H.J. Park, C. Kwak, Angew. Chem. Int. Ed. 50 (2011) 1792–1797.
[6] E.P. Murray, T. Tsai, S.A. Barnett, Nature 400 (1999) 649–651.
[7] T. Suzuki, T. Yamaguchi, K. Hamamoto, Y. Fujishiro, M. Awanoa, N. Sammes, Energy Environ. Sci. 4 (2011) 940–943.
[8] S.W. Tao, J.T.S. Irvine, Nat. Mater. 2 (2003) 320–323.
[9] H. Kan, H. Lee, Appl. Catal. B Environ. 97 (2010) 108–114.
[10] Y.H. Huang, R.I. Dass, Z.L. Xing, J.B. Goodenough, Science 312 (2006) 254–257.
[11] S. McIntosh, J.M. Vohs, R.J. Gorte, J. Electrochem. Soc. 150 (2003) A470–A476.
[12] X.J. Chen, K.A. Khor, S.H. Chan, Electrochem. Solid-state Lett. 8 (2005) A79–A82.
[13] M. Pillai, Y.B. Lin, H.Y. Zhu, R.J. Kee, S.A. Barnett, J. Power Sources 195 (2010) 271–279.
[14] K. Nikooyeh, R. Clemmer, V. Alzate-Restrepo, J.M. Hill, Appl. Catal. A: Gen. 347 (2008) 106–111.
[15] J.J. Guo, H. Lou, L.Y. Mo, X.M. Zheng, J. Mol. Catal. A: Chem. 316 (2010) 1–7.
[16] Z.Y. Hou, O. Yokota, T. Tanaka, T. Yashima, Appl. Catal. A: Gen. 253 (2003) 381–387.
[17] L.L. Xu, H.L. Song, L.J. Chou, Appl. Catal. B: Environ. 108, 109 (2011) 177–190.
[18] T. Horiuchi, K. Sakuma, T. Fukui, Y. Kubo, T. Osaki, T. Mori, Appl. Catal. A: Gen. 144 (1996) 111–120.
[19] D.L. Trimm, Catal. Today 49 (1999) 3–10.
[20] J. Sehested, Catal. Today 111 (2006) 103–110.
[21] J. Rostrup-Nielsen, D.L. Trimm, J. Catal. 48 (1977) 155–165.
[22] L. Ni, K. Kuroda, L.-P. Zhou, K. Ohta, K. Matsuishi, J. Nakamura, Carbon 47 (2009) 3054–3062.
[23] R. Bouarab, O. Akdim, A. Auroux, O. Cherifi, C. Mirodatos, Appl. Catal. A: Gen. 264 (2004) 161–168.
[24] A. Nandini, K.K. Pant, S.C. Dhingra, Appl. Catal. A: Gen. 290 (2005) 166–174.
[25] A.E.C. Luna, M.E. Iriarte, Appl. Catal. A: Gen. 343 (2008) 10–15.
[26] G. Bagnasco, J. Catal. 159 (1996) 249–252.
[27] G.V.A. Martins, G. Berlier, C. Bisio, S. Coluccia, H.O. Pastore, L. Marchese, J. Phys. Chem. C 112 (2008) 7193–7200.
[28] W. Wang, C. Su, Y.Z. Wu, R. Ran, Z.P. Shao, J. Power Sources 195 (2010) 402–411.
[29] J. Zhang, H.Y. Xu, X.L. Jin, Q.J. Ge, W.Z. Li, Appl. Catal. A: Gen. 290 (2005) 87–96.
[30] A.C. Ferrari, J. Robertson, Phys. Rev. B 61 (2000) 14095–14107.
[31] A. Cuesta, P. Dhamelincourt, J. Laureyns, A. Martinez-Alonso, J.M.D. Tascon, Carbon 32 (1994) 1523–1532.
[32] S.P. Jiang, S.P.S. Badwal, J. Electrochem. Soc. 144 (1997) 3777–3784.
[33] A. Bieberle, L.P. Meier, L.J. Gauckler, J. Electrochem. Soc. 148 (2001) A646–A656.
[34] W. Wang, R. Ran, C. Su, Z.P. Shao, D.W. Jung, S. Seo, S.M. Lee, Int. J. Hydrogen Energy 36 (2011) 10958–10967.
[35] R.D. Farr, C.G. Vayenas, J. Electrochem. Soc. 127 (1980) 1478–1483.